

Deep learning based on Transformer architecture for power system short-term voltage stability assessment with class imbalance

Yang Li^{a,*}, Jiting Cao^b, Yan Xu^c, Lipeng Zhu^d, Zhao Yang Dong^{c,*}

^a School of Electrical Engineering, Northeast Electric Power University, Jilin 132012, China

^b State Grid Chengde Power Supply Company, Chengde 067000, China

^c School of Electrical and Electronic Engineering, Nanyang Technological University, 639798, Singapore

^d College of Electrical and Information Engineering, Hunan University, Changsha, China

* Corresponding author. E-mail address: liyang@neepu.edu.cn (Y. Li), zy.dong@ntu.edu.sg (Z.Y. Dong).

Abstract: Most existing data-driven power system short-term voltage stability assessment (STVSA) approaches presume class-balanced input data. However, in practical applications, the occurrence of short-term voltage instability following a disturbance is minimal, leading to a significant class imbalance problem and a consequent decline in classifier performance. This work proposes a Transformer-based STVSA method to address this challenge. By utilizing the basic Transformer architecture, a stability assessment Transformer (StaaT) is developed as a classification model to reflect the correlation between the operational states of the system and the resulting stability outcomes. To combat the negative impact of imbalanced datasets, this work employs a conditional Wasserstein generative adversarial network with gradient penalty (CWGAN-GP) for synthetic data generation, aiding in the creation of a balanced, representative training set for the classifier. Semi-supervised clustering learning is implemented to enhance clustering quality, addressing the lack of a unified quantitative criterion for short-term voltage stability. Numerical tests on the IEEE 39-bus test system extensively demonstrate that the proposed method exhibits robust performance under class imbalances up to 100:1 and noisy environments, and maintains consistent effectiveness even with an increased penetration of renewable energy. Comparative results reveal that the CWGAN-GP generates more balanced datasets than traditional oversampling methods and that the StaaT outperforms other deep learning algorithms. This study presents a compelling solution for real-world STVSA applications that often face class imbalance and data noise challenges.

Keywords: Power system, short-term voltage stability assessment, Transformer architecture, class imbalance, renewable energy penetration, conditional Wasserstein generative adversarial network with gradient penalty (CWGAN-GP).

Word count: 5945.

Nomenclature

Abbreviations

STVS	Short-term voltage stability
STVSA	Short-term voltage stability assessment
TDS	Time-domain simulation
PMU	Phasor measurement units
DT	Decision tree
TS	Time series
ELM	Extreme learning machine
CNN	Convolutional neural network
GCN	Graph convolutional network
LSTM	Long-short term memory
GAN	Generative adversarial network
BiGRU	Bi-directional gated recurrent unit
StaaT	Stability assessment Transformer
SMOTE	Synthetic minority oversampling technique
ROS	Random oversampling
ADASYN	Adaptive synthetic
WGAN	Wasserstein GAN
WGAN-GP	WGAN with gradient penalty
CWGAN-GP	Conditional WGAN-GP

SFCM	Semi-supervised fuzzy C-means
CGAN	Conditional generative adversarial network
FC	Fully connected
SC	Silhouette coefficient
ACC	Accuracy
Mis	Misdetection
Fal	False-alarm
MCC	Matthews correlation coefficient
WD	Wasserstein distance
MMD	Maximum mean difference
FID	Fréchet incidence distance
COP-k-means	Constraint-partitioning k-means
OTW	Observation time window
SNR	Signal-to-noise ratio

Notations/Symbols

X	Dataset with all samples
N	The dimension of dataset X
m	The number of samples in X
C	The number of clusters
x_i	The i th sample in X
S_j	Fuzzy membership
J	Objective function of SFCM
u_{ij}	The extent to which sample x_i is affiliated with category j
c_j	The j th cluster center
c_s	The s th cluster center
l	Exponent weight
G	Generator
D	Discriminator
x	Real data
z	Noise
y	Label
\mathcal{D}	The set of 1-Lipschitz functions
\tilde{x}	Generated data
\hat{x}	Interpolation between x and \tilde{x}
P_r	Probability distributions followed by real data
P_z	Probability distributions followed by noise
P_g	Probability distributions followed by generated data
$P_{\hat{x}}$	Probability distributions followed by \hat{x}
γ	Possible joint distributions combined by P_r and P_g
$\ f\ _L$	Lipschitz constant of the function f
k	A constant serving as the upper bound for the $\ f\ _L$
λ	Gradient penalty coefficient
Q	Input feature matrix for queries
K	Input feature matrix for keys
V	Input feature matrix for values
d_K	The dimension of K
W^Q	Weight matrix for Q
W^K	Weight matrix for K
W^V	Weight matrix for V
W^O	Output weight matrix applied to the concatenated result of all heads
U	Voltage amplitude
P	Active power
Q_r	Reactive power
S	Time series dataset
n	The number of all subsets in dataset S
L	The number of system buses

S_h	The h th subset in S
d	The dimension of S_h
$f()$	A continuous function of x
$V(D, G)$	Objective function of GAN
$L(G)$	Critical loss of the G
$L(D)$	Critical loss of the D
$\ x_i - c_j\ $	Distance from x_i to c_j
$\mathbb{E}_{x \sim P_r}$	Expected value of P_r
$\Pi(P_r, P_g)$	The set of all possible joint distributions combined by P_r and P_g
$\inf_{\gamma \in \Pi(P_r, P_g)} \mathbb{E}_{(x, \tilde{x}) \sim \gamma} [\ x - \tilde{x}\]$	Lower bound of the expected value of the distance between samples x and \tilde{x}
$\ \cdot\ _2$	2-norm

<i>Units</i>	
s	Seconds
dB	Decibel
%	Percent

I Introduction

Short-term voltage stability (STVS) of power systems signifies their capacity to recover their voltages to an acceptable range following a disturbance, a crucial characteristic linked to the systems' stability [1]. With the swift escalation in electricity demand coupled with an inadequately expanded transmission system, the power system is often pushed to operate near its stability threshold, which increasingly threatens the secure operation of the system. The problem is further intensified by the escalating prevalence of induction motor loads [2] and the growing penetration of renewable energy [3], both of which significantly compound the challenge of maintaining short-term voltage stability in power systems [4].

To prevent a severe voltage dip during large disturbances, it is crucial to assess power system STVS. Specifically, the system's ability to maintain short-term voltage stability after a short-term large disturbance needs to be determined. Thus, the short-term voltage stability assessment (STVSA) issue is receiving widespread attention. Early research on STVSA mostly started from the physical mechanism, including the load dynamics of induction motors. Kawabe et al. [5] proposed a STVS analysis method based on the P-V plane, assessing the STVS by checking the state of the induction motor. Similarly, a scalable dynamic load model based on bifurcation theory for assessing the STVS in large-scale power systems is proposed in the work of Stanković et al. [6]. The primary approach for model-driven STVSA predominantly involves time-domain simulation (TDS). However, the short duration of transient processes combined with the large scale of power systems complicates the provision of timely information about STVS through model-driven methods [7]. Owing to the advent of wide-area measurement systems, phasor measurement units (PMUs) have gained prominence due to their capability to acquire large volumes of high-precision synchronized measurements. Consequently, these advancements have led to the widespread adoption of data-driven methods for stability assessment [8]. Reference [9] introduced a model-free STVSA approach utilizing the Lyapunov exponent. However, obtaining reliable results may become challenging when the Lyapunov exponent approximates zero. Utilizing PMU data, shallow machine learning has proven to be beneficial in the area of STVSA. In reference [10], the authors proposed a machine learning-based method for multi-state STVS classification, demonstrating low classification error and strong predictive capabilities. Further, the work of Zhu et al. [11] demonstrated an online STVSA method that amalgamated decision tree (DT) and time series (TS) classification using shapelets. Duchesne et al. [12] provided a detailed introduction to the principles of applying machine learning to the stability assessment of power systems. Reference [13] presented a hierarchical adaptive data analysis by using an extreme learning machine (ELM) to conduct real-time STVSA. This ELM-based approach is capable of analyzing not just voltage instability, but also fault-induced delayed voltage recovery. Building upon this, Zhang et al. [14] proposed a real-time STVSA method that can withstand data loss, enabling STVSA even in scenarios of PMU data loss. Lastly, the work of Lashgari et al. [15] proposed a fast DT-based machine learning scheme for timely and accurate prediction of voltage stability and identification of instability drivers.

With the continuous evolution of deep learning techniques, several deep learning models have been deployed to assess the STVS of power systems. For instance, Hagmar et al. [16] developed a supplementary warning system based on long short-term memory (LSTM), leveraging both real-time and historic data to accurately predict voltage instability minutes into the future, while Huang et al. [17] employed a convolutional neural network (CNN) for STVSA. Meanwhile, another study [18] proposed a STVSA method combining graph convolutional networks (GCNs) and LSTM to capture both temporal and spatial features. In a similar vein, Luo et al. [19] extracted spatial features via GCN and deployed one-dimensional convolution networks to learn temporal information. Furthermore, the work of Zhu et al. [20] employed LSTM to determine the STVS of power systems and proposed intelligent assessment schemes. Finally, reference [21] adopted a generative adversarial network (GAN) to enhance the sample and assess STVS utilizing a bi-directional gated recurrent unit (BiGRU). However, LSTMs are not designed for parallel computing and tend to struggle with processing long sequence data. In contrast, CNNs can handle parallel computation

effectively, but they are less capable when it comes to managing long-distance dependencies within the data. The inherent limitations of these algorithms prevent them from satisfying the requirements for the rapid processing of features that span long distances in data sequences. This need is accentuated by the increasing complexity of power systems, thereby compromising the assessment performance significantly [22]. Within the field of computer vision, the Transformer model, as highlighted in reference [23], disrupted the traditional reliance of deep learning on CNNs and recurrent neural networks (RNNs), and in doing so, established an encoder-decoder model exclusively grounded in self-attention mechanisms. Beyond this, the Transformer has found wide-ranging applications, including but not limited to load forecasting [24] and forced oscillation localization in power systems [25]. Consequently, this study simplifies the Transformer, incorporates it into STVSA, and puts forth the stability assessment Transformer (StaaT).

In existing research on STVSA in power systems, the substantial amount of required data is typically generated by simulations [21], [26]. During this process, the errors of the used model and its parameters are inevitable. Enhancing the reliability of the assessment model becomes significantly feasible when the measured data is procured from actual PMUs. However, the real post-disturbance system tends to be predominantly stable, resulting in a serious imbalance in the stable-to-unstable ratio. If not addressed appropriately, this sort of class imbalance problem can severely undermine the performance of the model [27]. In the STVSA field, reference [28] utilized a hybrid method that combines oversampling with cost-sensitive learning. This strategy not only considers the degree of imbalance but also weighs the cost of misclassification. Nonetheless, cost-sensitive learning necessitates the use of expert knowledge for meticulously establishing the cost matrix. Given the escalating complexity of application problems and the potential constraints stemming from experts' experience and knowledge, the accuracy of the cost matrix may be compromised. In general, data resampling serves as the most prevalent approach to achieving a balanced sample distribution [28]. Data resampling techniques primarily include oversampling, undersampling, and mixed sampling. Classic oversampling techniques such as synthetic minority oversampling technique (SMOTE), random oversampling (ROS), and adaptive synthetic (ADASYN) sampling have been widely used. However, these techniques are not without their limitations. For example, linear oversampling methods like SMOTE and ROS are prone to overfitting, while ADASYN is susceptible to outliers. The GAN, proposed in reference [29], is extensively utilized for data resampling, primarily due to the authenticity and diversity of its generated samples. However, conventional GANs grapple with training difficulties and the need for careful coordination of generator and discriminator parameters. To mitigate these challenges, the Wasserstein GAN (WGAN) was introduced in reference [30]. Subsequently, reference [31] proposed the Wasserstein GAN with gradient penalty (WGAN-GP) to prevent gradient vanishing in WGAN. The current study utilizes a conditional WGAN-GP (CWGAN-GP) to tackle the class imbalance problem in STVSA. This marks a significant advancement over existing methods with known drawbacks, such as the propensity for overfitting in SMOTE and ROS, and sensitivity to outliers in ADASYN. The proposed CWGAN-GP not only addresses these limitations but also optimizes the neural network's learning capacity by ensuring uniform weight distribution. The method relies on balanced datasets generated by CWGAN-GP for model training, thereby circumventing the deterioration of deep learning model performance caused by class imbalance during training.

To underscore the limitations of existing methodologies and the novelty of this study, a comparison and analysis of the most recent research in the field of data-driven STVSA has been conducted. The findings are presented in Table I.

TABLE I
COMPARISON OF CURRENT STUDY WITH PREVIOUS RESEARCH IN DATA-DRIVEN STVSA

Reference	Class imbalance	Imbalanced learning method	Deep learning	Self-attention mechanism
[32]	—	—	—	—
[13]	—	—	—	—
[14]	—	—	—	—
[17]	—	—	✓	—
[18]	—	—	✓	—
[19]	—	—	✓	—
[20]	—	—	✓	—
[28]	✓	oversampling, cost-sensitive learning	—	—
[33]	—	—	✓	—
This paper	✓	generative adversarial network	✓	✓

Considering all the issues discussed, a STVSA method is proposed based on CWGAN-GP and StaaT in environments with class imbalance. This work's principal contributions include:

- 1) The imbalance learning method based on CWGAN-GP is proposed to address the class imbalance problem in STVSA. Unlike the oversampling method that generates samples by simple linear sampling, this technique generates a balanced, realistic dataset from real data. Moreover, the method proves resilient under class imbalances up to 100:1, beyond which its effectiveness decreases, underscoring its practicality in dealing with real-world data imbalance challenges.
- 2) This study designs a STVSA model based on stability assessment Transformer. This model leverages its multi-head self-attention mechanism to enhance efficiency through parallel computing, enabling it to simultaneously learn the characteristics of different positions in the time series samples.

- 3) An additional contribution of this study lies in demonstrating that the proposed method maintains robust performance even in scenarios with increased penetration of renewable energy. The exploration of how renewable energy integration impacts the STVSA enriches the understanding of complex post-disturbance dynamics and stability boundaries in power systems, thereby enhancing the method's practical applicability.

The suggested approach undergoes testing on the IEEE 39-bus test system under class imbalance conditions. In the test, various statistical indexes were selected for testing. Experimental results indicate a superior performance of the proposed method over alternatives. Moreover, this study conducts a sensitivity analysis on the parameters that may affect the results.

II Related algorithms

A. Semi-supervised Clustering Algorithm

A significant challenge within the realm of STVSA is the absence of a uniform quantitative criterion, making the process of acquiring accurate sample labels complex. The consecutive labeling of all training samples, when relying solely on domain knowledge, can potentially lead to inefficiencies. However, depending exclusively on unsupervised learning with unlabeled data may yield inconsistent results. Fortunately, the well-understood concept of voltage stability can offer crucial insights. For instance, as outlined by reference [11], if none of the bus voltages drop below 0.9 pu for a period of 10 seconds, the system can be confidently categorized as stable; in contrast, a definitive label of instability can be assigned if all bus voltages drop below 0.7 pu without recovery. This clear understanding allows for the accurate labeling of a small subset of samples, which can subsequently serve as prior information for clustering the remaining unlabeled samples. Therefore, this study employs a semi-supervised clustering algorithm to enhance the sample labeling process.

Based on these clearly labeled samples, the semi-supervised fuzzy C-means (SFCM) method can be used to judge the stability of each sample. An N -dimensional dataset $X = x_i (1 \leq i \leq m)$ is divided into C clusters, and each sample belongs to clusters through fuzzy membership $S_j (1 \leq j \leq C)$. In semi-supervised learning, these labeled samples in X function as prior knowledge. The SFCM algorithm leverages this information from labeled data to guide the process of iterative optimization of the overall clustering. The objective function J of SFCM is

$$J = \sum_{i=1}^m \sum_{j=1}^C u_{ij}^l \|x_i - c_j\|^2 \quad (1)$$

where u_{ij} indicates the extent to which sample x_i is affiliated with category j ; l denotes the exponent weight; c_j is the j th cluster center; and $\|x_i - c_j\|$ represents the distance from x_i to c_j . The specific representations of the degree of membership u_{ij} and the cluster center c_j are

$$u_{ij} = \frac{1}{\sum_{s=1}^C \left(\frac{\|x_i - c_j\|}{\|x_i - c_s\|} \right)^{\frac{1}{l-1}}} \quad (2)$$

$$c_j = \frac{\sum_{i=1}^m u_{ij}^l \cdot x_i}{\sum_{i=1}^m u_{ij}^l} \quad (3)$$

where c_s refers to the s th cluster center. Due to space constraints, the specific steps of the SFCM will not be elaborated further. For more details on SFCM, please refer to references [21], [34].

B. Conditional Wasserstein GAN with Gradient Penalty

In recent years, GANs have played a crucial role in data resampling, generating renewable scenarios [35], and addressing renewable output uncertainties in economic dispatch problems [36]. The generator's objective is to produce an ample number of denoted samples, while the discriminator's mission is to distinguish between generated and real samples with the highest possible accuracy. Through this dynamic competition, they mutually constrain and evolve. As a result, the generated samples more closely resemble the real ones, thus obtaining the desired samples. The objective function $V(D, G)$ of GAN is

$$\min_G \max_D V(D, G) = \mathbb{E}_{x \sim P_r} [\log D(x)] + \mathbb{E}_{z \sim P_z} [\log(1 - D(G(z)))] \quad (4)$$

where G denotes the generator, while D stands for the discriminator. Noise is denoted by z , whereas P_r and P_z are the probability distributions followed by real data x and noise z respectively. The expected value is given by $\mathbb{E}_{x \sim P_r}$. Random noise is fed into the generator to generate synthetic data, which is then input into the discriminator alongside the real data. The discriminator's job is to determine the authenticity of the input. When real samples are inputted, the result inclines towards 1, while with fake samples, it leans towards 0. Through training, when either real or generated samples are fed into the system, the outcome of $V(D, G)$ is 0.5, indicating that the generator can, at this point, create convincingly real pseudo-samples.

The conditional GAN (CGAN) , an extension of GAN [37], has the following objective function:

$$\min_G \max_D V(D, G) = \mathbb{E}_{x \sim P_r} [\log D(x | y)] + \mathbb{E}_{z \sim P_z} [\log(1 - D(G(z) | y))] \quad (5)$$

where y can be any type of additional information.

However, the original GAN has inadequacies in training and needs to carefully coordinate the training level of G and D [38]. To address this concern, WGAN was proposed in [30], and an approach to removing $\log()$ from the objective functions of G and D was suggested, expressed as

$$\min_G \max_{D \in \mathcal{D}} V(D, G) = \mathbb{E}_{x \sim P_r} [D(x)] + \mathbb{E}_{z \sim P_z} [1 - D(G(z))] \quad (6)$$

where \mathcal{D} represents the collection of 1-Lipschitz functions. By using the D of WGAN to fit distance instead of classification, the discriminator of the original GAN performs a dual-classification task. Thus, the sigmoid function of the last layer of D is removed. The study also indicates that if two distributions do not overlap or the overlap is negligible in a high-dimensional space, Kullback–Leibler divergence and Jensen–Shannon divergence can neither reflect the distance nor provide the gradient. The recommended metric for providing a meaningful gradient is the original Wasserstein distance, defined as follows:

$$W(P_r, P_g) = \inf_{\gamma \in \Pi(P_r, P_g)} \mathbb{E}_{(x, \tilde{x}) \sim \gamma} [\|x - \tilde{x}\|] \quad (7)$$

where P_g denotes the probability distributions of generated data; $\Pi(P_r, P_g)$ is the set of all possible joint distributions combined by P_r and P_g . For each possible joint distribution γ , real data x and generated data \tilde{x} can be derived from $(x, \tilde{x}) \sim \gamma$. The lower bound $\inf_{\gamma \in \Pi(P_r, P_g)} \mathbb{E}_{(x, \tilde{x}) \sim \gamma} [\|x - \tilde{x}\|]$ of the expected value of the sample distance in all possible joint distributions is defined as Wasserstein distance. As $\inf_{\gamma \in \Pi(P_r, P_g)}$ cannot be solved directly, it was transformed into [30]:

$$W(P_r, P_g) = \frac{1}{k} \sup_{\|f\|_L \leq k} \mathbb{E}_{x \sim P_r} [f(x)] - \mathbb{E}_{x \sim P_g} [f(x)] \quad (8)$$

where $f(x)$ is a continuous function of x , $\|f\|_L$ denotes the Lipschitz constant of the function f , and the function f is referred to as a k -Lipschitz function if it satisfies $\|f\|_L \leq k$ for some constant k . To satisfy $\|f\|_L \leq k$, each time the parameters of D are updated in WGAN, their absolute values are truncated to no more than a fixed constant. However, reference [31] suggested that in WGAN, if the threshold c , a key parameter constraining the discriminator’s weights, is not fine-tuned, issues like gradient disappearance or explosion may occur. The critical losses of the G and D of WGAN-GP are given by [31]:

$$L(G) = \mathbb{E}_{\tilde{x} \sim P_g} [D(\tilde{x})] \quad (9)$$

$$L(D) = \mathbb{E}_{\tilde{x} \sim P_g} [D(\tilde{x})] - \mathbb{E}_{x \sim P_r} [D(x)] + \lambda \mathbb{E}_{\hat{x} \sim P_{\hat{x}}} [\|\nabla_{\hat{x}} D(\hat{x})\|_2 - 1]^2] \quad (10)$$

where \hat{x} is an interpolation between x and \tilde{x} , $P_{\hat{x}}$ represents the probability distributions followed by \hat{x} , $\|\cdot\|_2$ denotes the 2-norm, and λ is the gradient penalty coefficient. The gradient penalty is independently applied to each sample to ensure that $G(z)$ is close to x , and the approaching process $D(G(z))$ does not exceed $D(x)$. In CWGAN-GP, the objective function can be defined as follows:

$$\min_G \max_D V(D, G) = \mathbb{E}_{x \sim P_r} [D(x | y)] - \mathbb{E}_{\tilde{x} \sim P_g} [D(\tilde{x} | y)] - \lambda \mathbb{E}_{\hat{x} \sim P_{\hat{x}}} [(\|\nabla_{\hat{x}} D(\hat{x} | y)\|_2 - 1)^2] \quad (11)$$

C. Transformer

The Transformer, along with its enhanced variants, fundamentally represents a sequence-to-sequence architecture. This is primarily composed of two significant components: the encoder and the decoder. Within the encoder, multiple identical layers are stacked, each of which includes the multi-head self-attention mechanism and the feed-forward neural network (FNN). The decoder enriches the original design by introducing an encoder-decoder attention sublayer on top of the multi-head self-attention and FNN of the encoder. Further, every sub-layer is complemented with a residual connection and layer normalization. To preserve the input order for the model, the Transformer incorporates a position code at the input layer.

The self-attention mechanism treats the sequence by substituting each element with the weighted mean of the remainder of the sequence. While attention mechanisms have found application across diverse domains, reference [23] introduced the concept of ‘‘Scaled Dot-Product Attention’’. The complete formula is written as

$$\text{Attention}(Q, K, V) = \text{softmax}\left(\frac{QK^T}{\sqrt{d_K}}\right)V \quad (12)$$

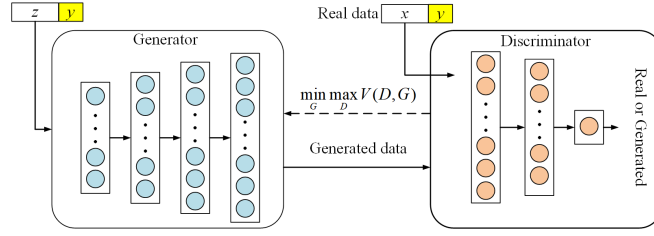


Fig. 1. Structure of CWGAN-GP.

where Q , K , and V are the input feature matrices for queries, keys, and values, respectively, while d_K denotes the dimension of the keys matrix, K . Reference [23] further proposed the idea of multi-head attention, which essentially processes input features from distinct positions through different weights to derive the final result. The formula is as follows:

$$\text{MultiHead}(Q, K, V) = \text{Concat}(\text{head}_1, \dots, \text{head}_h) W^O \quad (13)$$

$$\text{where head}_i = \text{Attention}(QW_i^Q, KW_i^K, VW_i^V)$$

where W^Q , W^K , and W^V are the weight matrices for query, key, and value, respectively, and W^O is the output weight matrix applied to the concatenated result of all heads. The multi-head attention mechanism empowers the Transformer model to glean information from diverse locations, thus offering an advantage over the single attention mechanism.

III Class imbalance learning based on CWGAN-GP

A. Model structure

In this study, the CWGAN-GP structure encompasses a generator and a discriminator, as illustrated in Fig. 1. The generator is constructed as a 4-layer fully connected (FC) network. Meanwhile, the discriminator is designed as a three-layer FC network, with each layer comprising 512, 256, and 1 neuron, respectively. The activation function utilized in both the generator and discriminator is LeakyReLU. To train the classifier, the generated samples are employed as the training set. These samples, generated by the CWGAN-GP model, serve as input data to train the classifier, allowing it to learn and generalize from the generated data.

B. Model training process

The model training process of CWGAN-GP is divided into three steps.

Step 1: Random noise, denoted as z , and labels, represented by y , are fed into the generator. The generator is trained to produce generated samples that align with the distribution of real samples.

Step 2: The generated data and real data are randomly mixed together and input into the discriminator. The discriminator then evaluates the probability of each sample being real or fake.

Step 3: Through repeated iterations and optimization, a trained generator is obtained. This trained generator is capable of generating a balanced training set, which can be further utilized for STVSA.

IV Proposed STVSA model

A. Stability assessment Transformer

When Transformer is applied in natural language processing, the encoder layer is responsible for learning data features, while the decoder layer utilizes these learned features for prediction. However, in the specific case of a classification task, the focus lies solely on learning the data features. Consequently, this study modifies the original Transformer architecture by removing the decoder layer. Instead, it directly connects the FC layer and Softmax function after multiple encoder layers to generate the final model results. This simplified version of Transformer is specifically adapted for STVSA purposes. The structure diagram of StaaT is illustrated in Fig. 2.

The input to StaaT consists of a TS sample comprising real-time power system data collected by PMUs. The positional embedding technique is employed to encode the data's positional information before it is forwarded to the encoder. Within each layer of the encoder, the multi-head attention mechanism facilitates the learning of data features through self-attention. The learned features are then propagated back through the FNN. The final layer of the encoder outputs the results through a FC layer followed by a Softmax function, determining whether the sample is classified as stable or not.

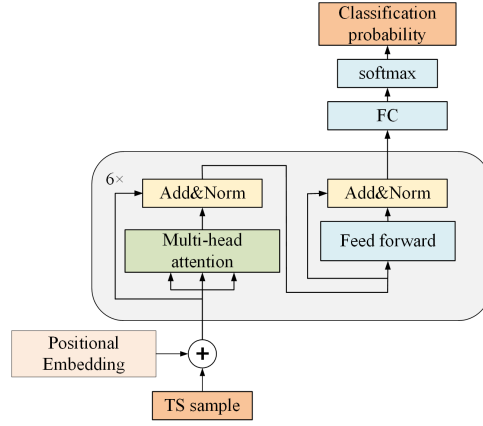


Fig. 2. Structure diagram of StaaT.

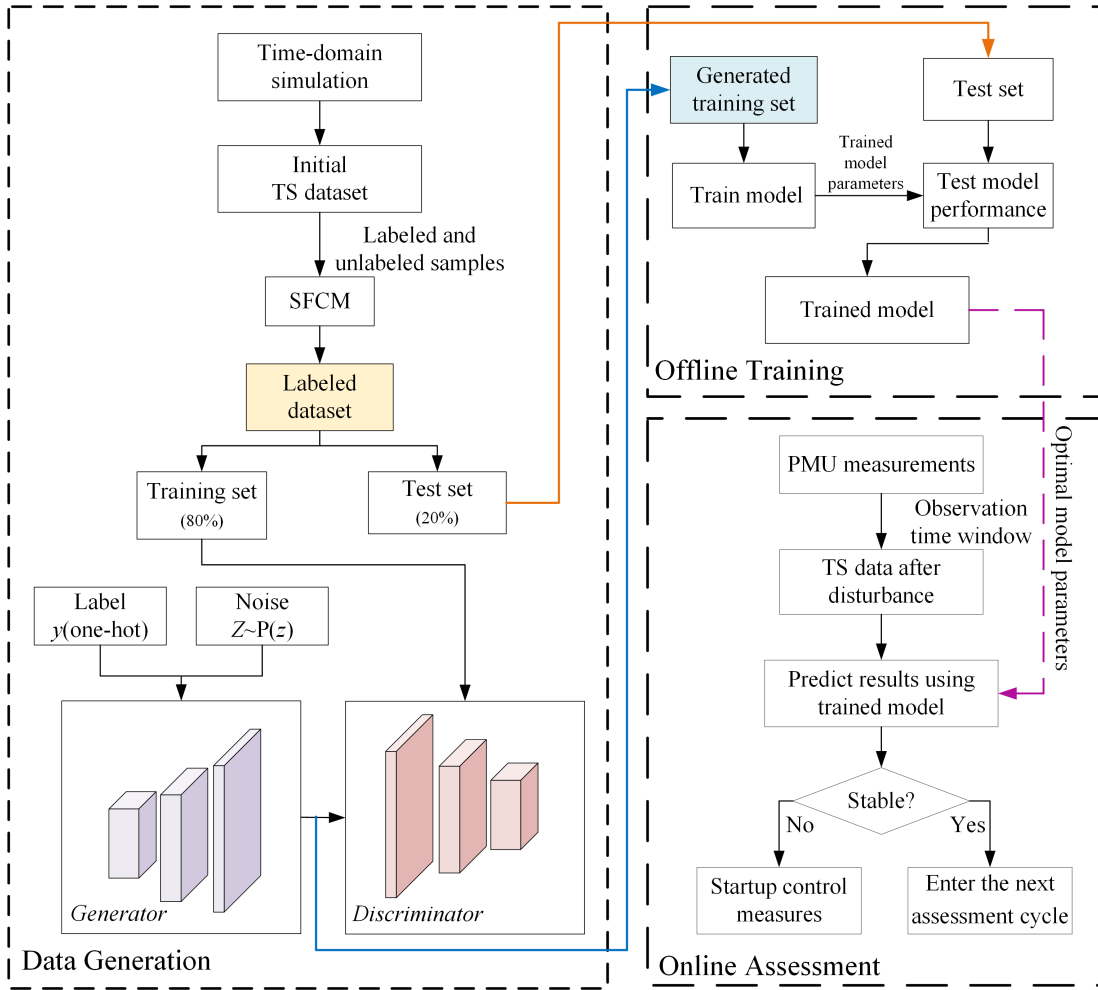


Fig. 3. Flowchart of the proposed method.

B. STVSA processes

The proposed STVSA scheme in this study consists of three stages, as depicted in Fig. 3.

First stage: Data generation. Considering different operating conditions in the time-domain simulation, the initial TS samples comprising normalized voltage amplitude (U), active power (P), and reactive power (Q_r) of each bus within a short time period after fault clearance can be obtained [19]. Subsequently, the unlabeled ones in the initial sample dataset are labeled using SFCM, resulting in a fully labeled dataset. This dataset is subsequently partitioned into training and test sets using a 4:1 ratio [11], with the training set serving as input for the CWGAN-GP model, which generates a balanced training set.

Second stage: Offline training. The generated training set is utilized to train the StaaT model, while the test set is employed to evaluate its performance. The optimal parameters obtained from the trained model are saved for subsequent online assessments.

Third stage: Online assessment. Once a big disturbance occurs in the power system, electrical quantities U , P , and Q_r will be captured in real-time by PMUs and transmitted to the trained StaaT model for assessing the system's stability outcomes. If the system is classified as stable, the monitoring process continues. However, if the system is identified as unstable, appropriate control measures are promptly initiated to mitigate the impact of short-term voltage instability.

C. Assessment indicators

1) Silhouette coefficient

This study uses silhouette coefficient (SC) as an index of the clustering algorithm [21], defined as

$$SC = \frac{1}{N} \sum_{j=1}^N \frac{b_j - a_j}{\max(a_j, b_j)} \quad (14)$$

where $x_j (1 \leq j \leq N)$ is a sample in the dataset with N samples; a_j denotes the average distance of sample x_j from all other samples in the same cluster, reflecting the degree of aggregation of this cluster; b_j denotes the minimum average distance from x_j to all other clusters, reflecting the degree of separation between different clusters.

2) Statistical indexes for classification

In the context of data-driven STVSA, the misclassification of an unstable sample as stable can precipitate serious consequences, such as voltage collapse, due to the system's failure to initiate the necessary control measures. Given the varied costs associated with misclassification, the reliance solely on accuracy (ACC) [21], [39] proves inadequate for comprehensive STVSA. It is crucial to employ additional statistical tests, such as the F1-score [21], [39], misdetection (Mis) [8], [28], false-alarm (Fal) [8], [28], and G-mean [28], to comprehensively evaluate the performance. By considering these additional statistical tests, a more comprehensive assessment of the STVSA model's performance can be achieved, ensuring effective detection of unstable samples and minimizing the risks associated with misjudgment.

3) Evaluation indicators of GAN

This paper adopts Wasserstein distance (WD) [21], maximum mean difference (MMD) [40], and Fréchet incidence distance (FID) [41] as quantitative evaluation metrics to assess the performance of CWGAN-GP. A lower value for each of these metrics indicates better model performance. The precise definitions of these three indicators can be found in the references mentioned earlier.

V Case study

The tests in this study are performed on the IEEE 39-bus test system, a well-known system in STVSA [21], [33], [42], as depicted in Fig. 4. The generator in the system is equipped with a third-order exciter model, and further details can be found in [43]. The dataset is obtained using commercial simulation software, PSD-BPA, which effectively enables accurate simulations and facilitates the acquisition of data for the experiments. The implementation of the proposed approach is achieved by using PyTorch 1.7 and Tensorflow 1.14 within the Python 3.7 environment. The developed programs are deployed on a personal computer with the following specifications: Intel Core i5-6300HQ 2.3GHz CPU, 4GB RAM, and GTX 960M GPU. These hardware and software configurations facilitate efficient execution of the algorithm and enable comprehensive analysis of the results.

The main hyperparameters of CWGAN-GP and StaaT are presented in Table II and Table III respectively. These hyperparameters have been selected via trial and error. In Table II, the parameter n_{critic} is used to strike a balance between the convergence speed of CWGAN-GP training.

TABLE II
HYPERPARAMENTS SETTING OF CWGAN-GP

Hyperparameters	Values
Gradient penalty factor	10
Optimizer	Adam
Learning rate	0.0001
Batch size	64
n_{critic}	5
Epoch	500

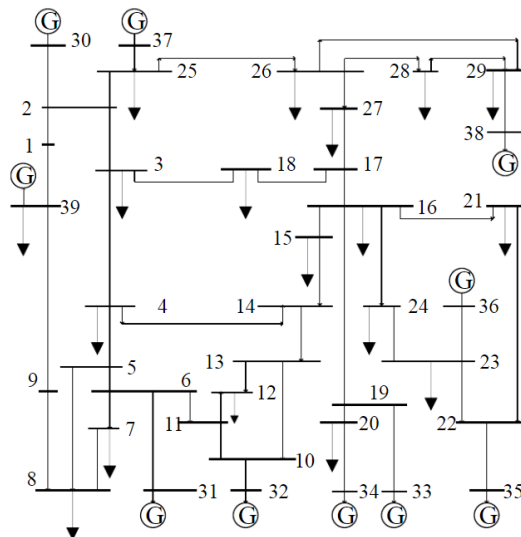


Fig. 4. One-line diagram of IEEE 39-bus test system

TABLE III
HYPERPARAMENTS SETTING OF STAAT

Hyperparameters	Values
The number of multi-head attention	8
Optimizer	Adam
Dropout	0.5
Learning rate	0.0001
Batch size	64
Epoch	200

A. Dataset generation

Short-term voltage instability, which often occurs following a fault, is predominantly linked to the rapid recovery of loads, especially those associated with induction motors [44], [45]. Hence, in the simulations, the load model of the power system is set up with induction motor load and static ZIP load [46]. As illustrated in Table IV, various operating conditions, induction motor load ratios, fault types, and fault locations are designated to simulate crucial operating conditions and emergencies.

TABLE IV
SIMULATION PARAMETERS FOR DATASET GENERATION

Type	Value
Load level	80%, 100%, 120%
Induction motor load ratio	70%, 80%, 90%
Fault type	three-phase short circuit
Fault location	0%, 25%, 50%, and 75% of the transmission lines
Fault clearing time	0.05 s at the near end; 0.1 s at the far end

With the configurations set forth in Table IV, real-time system data encompassing voltage amplitude, along with active and reactive power (symbolized as U , P , and Q_r) as per the study [19], are procured through time-domain simulation via PSD-BPA, thereby constructing the TS dataset S .

$$S = [S_1, S_2, \dots, S_h, \dots, S_n] (1 \leq h \leq n) \quad (15)$$

where n indicates that the dataset S consists of n subsets, and the specific composition is as follows:

$$S_h = [(U_1, \dots, U_L), (P_1, \dots, P_L), (Q_{r,1}, \dots, Q_{r,L})]_1, \dots, [(U_1, \dots, U_L), (P_1, \dots, P_L), (Q_{r,1}, \dots, Q_{r,L})]_d \quad (16)$$

where L represents the number of system buses, d is the dimension of S_h .

According to the settings in Table IV, a total of 5500 samples are generated in this paper, of which unstable samples account for 9.09% of the total samples.

B. Performance test of SFCM

According to the acceptance rules outlined in Section II-A, labels can be acquired for all data samples only in a minority of cases. The SFCM method incorporates a small subset of data samples with known labels as prior information and uses it within the SFCM objective function to perform clustering. Consequently, labels are derived for all data. Two distinct label sets are differentiated using constraint-partitioning k-means (COP-k-means) and the engineering criteria mentioned in [11]. To assess the efficacy of the SFCM method, the silhouette coefficients of these three label sets are calculated and used as performance indicators. The results are presented in Table V.

TABLE V
COMPARISON OF CLUSTERING EFFECTIVENESS

Index	SFCM	COP-k-means	Engineering criterion
<i>SC</i>	0.4874	0.3954	0.2682

The SFCM method produces satisfactory results in labeling samples, as shown in Table V. It demonstrates nearly double the efficiency compared to using the engineering criterion, and also exceeds the performance of the COP-k-means algorithm. These results highlight the superior efficiency of SFCM in clustering data samples.

C. Performance tests of CWGAN-GP

To assess the effectiveness of CWGAN-GP in dealing with class imbalance issues, this study employs several different data resampling algorithms, including SMOTE, ROS, and ADASYN, on the same initial dataset. The specific parameters for these methods are detailed in [47], [48], and [49], respectively. The assessment results obtained from StaaT are summarized in Table VI.

TABLE VI
PERFORMANCE COMPARISON OF CWGAN-GP AND DATA RESAMPLING METHODS

Data resampling method	ACC(%)	MCC	Mis(%)	Fal(%)	G-mean
ROS	98.87	0.9288	0.09	1.18	0.9885
SMOTE	98.91	0.9381	0.09	1.00	0.9895
ADASYN	99.09	0.9469	0.18	0.73	0.9860
CWGAN-GP	99.82	0.9892	0	0.18	0.9990

Table VI reveals that CWGAN-GP outperforms the data resampling algorithms, exhibiting superior performance across all indices. Particularly, the proposed method yields a zero misdetection rate, aligning more with engineering requirements. Furthermore, as alluded to earlier, the MCC offers a clearer representation of algorithm performance in resolving class imbalance. The MCC of CWGAN-GP notably exceeds those of other algorithms by a minimum of 0.04, suggesting that the data generated by CWGAN-GP can better address the issue.

To validate the data generation capabilities of CWGAN-GP, this study conducts a comparison with CGAN in terms of WD, MMD, and FID. The results of this comparison are depicted in Table VII.

TABLE VII
COMPARISON OF DATA GENERATION CAPABILITIES: CWGAN-GP VS CGAN

Indicators	CWGAN-GP	CGAN
WD	2.687	4.362
MMD	0.069	0.091
FID	1.448	2.276

As illustrated in Table VII, the WD, MMD, and FID metrics associated with CWGAN-GP surpass those of the CGAN. Notably, the WD for CWGAN-GP is 38.4% lower than that of CGAN, suggesting that CWGAN-GP is superior to CGAN in terms of data generation capabilities.

Aside from algorithmic differences, the proportion between positive and negative samples in the initial dataset can also influence the classifier's performance in addressing class imbalance issues. To investigate this, the proposed method is applied to process and evaluate the performance of the initial dataset with various proportions. The findings are presented in Table VIII.

All proposed methods, despite varying ratios of positive to negative samples, yield high-performing samples as demonstrated in Table VIII. Although the overall performance remains commendable when the ratio of positive to negative samples in the initial dataset increases, there is a slight decrease in performance. This demonstrates the robust adaptability of CWGAN-GP to varying ratios between positive and negative samples. Moreover, as the degree of category imbalance escalates, the performance

TABLE VIII
CLASSIFIER PERFORMANCE ACROSS VARIOUS POSITIVE TO NEGATIVE SAMPLE RATIOS

Proportions	ACC(%)	MCC	G-mean
5:1	99.83	0.9940	0.9970
10:1	99.82	0.9892	0.9990
50:1	99.61	0.8980	0.9477
100:1	99.60	0.7980	0.8935
200:1	99.55	0.5453	0.7734

of the proposed method initially remains relatively stable. However, when the degree of imbalance reaches 100:1, the efficiency of the investigated approach begins to degrade to an unacceptable level. Note that the metric ACC doesn't significantly fluctuate with increasing imbalance, which suggests it's not entirely reasonable to gauge the effectiveness of the suggested method solely based on accuracy.

D. Performance test at different observation times

The rapid nature of short-term voltage fluctuations necessitates immediate attention following any significant disruption. If data from shorter observation periods after a major disturbance could be utilized to accurately determine system stability, it would create more time for subsequent protective actions within the power system, thus ensuring better stability. To explore this concept, four different lengths for observation time windows (OTWs) are selected, and their respective accuracies are computed. The findings of this examination are compiled in Table IX.

TABLE IX
ACCURACIES AT DIFFERENT OBSERVATION TIMES

Lengths of OTW (s)	Training accuracy (%)	Testing accuracy (%)
0.03	99.88	99.82
0.04	99.81	99.78
0.05	99.79	99.73
0.06	99.89	99.82

As illustrated in Table IX, the model presents high accuracy when the length of OTW is 0.03 s. As this length increases, both the training and testing accuracies remain relatively stable. Given the balance between assessment speed and accuracy, a 0.03s OTW is adopted across all test examples.

E. Performance test of StaaT

In order to assess the performance of StaaT, the model is evaluated using a confusion matrix, as presented in Table X.

TABLE X
CONFUSION MATRIX

	Stable (Actual)	Unstable (Actual)
Stable (Predicted)	998	0
Unstable (Predicted)	2	100

As demonstrated in Table X, the StaaT registers a false alarm rate of merely 0.18%, and a misdetection rate hits 0%. These outcomes ensure the system's superior accuracy in instability assessments, aligning well with practical requirements. Consequently, the proposed method delivers dependable results and bears substantial practical relevance.

For a more comprehensive evaluation of StaaT, this study compares its test results with other prevalent classification models, namely LSTM, CNN, and BiGRU. The comparison encompasses four metrics: ACC, MCC, F1-score, and Mis. These benchmark algorithms also undergo parameter optimization via a trial and error approach. The summarised outcomes of these comparisons are presented in Table XI.

TABLE XI
PERFORMANCE COMPARISON OF STAAAT WITH OTHER CLASSIFICATION MODELS

Classification model	ACC(%)	MCC	F1-score	Mis(%)
LSTM	95.18	0.7179	0.9734	2.09
CNN	95.82	0.7565	0.9769	1.73
BiGRU	98.55	0.9171	0.9920	0.27
StaaT	99.82	0.9892	0.9990	0

As exhibited in Table XI, all the performance indicators of StaaT outshine those of the contrasted deep learning algorithms. Specifically, boasting the highest MCC and the smallest Mis, StaaT demonstrates superior performance in an environment of class imbalance. This is primarily attributed to the self-attentive mechanism of the StaaT model that allows for comprehensive learning of information at each data position, thereby rendering it more effective than the other alternatives such as CNN, LSTM, and BiGRU.

F. Performance test with renewable energy integration

As renewable energy units continue to merge into the power grid, the dynamic characteristics of the system following disturbances grow increasingly complex [50]. In order to assess the implications of renewable energy unit integration on the proposed methodology, this work examines its performance under varying rates of renewable energy penetration. The outcomes of these assessments are depicted in Table XII.

TABLE XII
PERFORMANCES OF THE PROPOSED APPROACH UNDER DIFFERENT RENEWABLE ENERGY PENETRATION RATES

Penetrations rates (%)	ACC(%)	MCC	Mis(%)	Fal(%)	G-mean
0	99.82	0.9892	0	0.18	0.9990
10	99.73	0.9836	0.09	0.18	0.9940
20	99.55	0.9726	0.18	0.27	0.9885
30	99.36	0.9617	0.27	0.36	0.9829

Based on the assessment outcomes presented in Table XII, it is evident that the performance of the proposed approach declines in proportion to the increasing penetration of renewable energy sources. This decrease can be attributed to the escalating complexity in post-disturbance dynamics as renewable energy sources are integrated into the power grid, making them more challenging to learn. Nonetheless, the proposed model sustains a commendable performance level even at a penetration rate as high as 30%. This strongly suggests that the proposed model is capable of delivering effective STVSA for power systems linked to renewable energy sources.

G. Robustness test under noisy environments

To assess the robustness of the StaaT model in noisy conditions, Gaussian white noises with varying signal-to-noise ratios (SNRs) are incorporated into the test dataset. However, in real-world scenarios, measurement noise is inevitable during the real-time sampling process conducted by PMUs. The performance under these test conditions is presented in Table XIII.

TABLE XIII
PERFORMANCE COMPARISON UNDER DIFFERENT SNRS

SNR (dB)	ACC (%)	MCC	Fal (%)	Mis (%)	G-mean
Noise-free	99.82	0.9892	0.18	0	0.9990
50	99.73	0.9836	0.18	0.09	0.9940
40	99.45	0.9678	0.45	0.09	0.9925
30	99.18	0.9527	0.73	0.09	0.9910

Table XIII demonstrates that, even under various SNR noise conditions, the proposed classifier maintains superior performance. Notably, an increase in the noise proportion does not significantly affect the classifier's performance. This stability under noise disturbance demonstrates the robustness of the proposed method.

VI Conclusion

To address the challenge of class imbalance in short-term voltage stability assessment, a novel approach has been developed in this study by leveraging the capabilities of CWGAN-GP and StaaT. The research findings are summarized as follows:

- 1) The proposed imbalance learning method based on CWGAN-GP effectively addresses the class imbalance problem in STVSA. The method generates a balanced, realistic dataset from real data and exhibits resilience under class imbalances up to 100:1. The superior performance of the CWGAN-GP is confirmed when compared with CGAN and several data resampling techniques, including SMOTE, ROS, and ADASYN.
- 2) The employment of StaaT for STVSA enables the extraction of the most important features in the dataset. Notably, it outperforms other alternative methods, demonstrating increased accuracy, improved Matthews Correlation Coefficient, superior F1-score, and minimized misclassification rates.
- 3) The proposed method demonstrates robust performance even under varying ratios of positive to negative samples and under noisy environments. Moreover, it maintains consistent effectiveness even in scenarios with increased penetration of

renewable energy, providing valuable insights into the understanding of complex post-disturbance dynamics in power systems.

Future work will consider real-world scenarios where missing PMU data may occur and extend the testing of the proposed method to larger power system models. Furthermore, combining the data-driven approach of this study with model-driven techniques might offer a comprehensive insight into the causes of voltage instability, thereby facilitating the development of effective corrective measures.

Acknowledgement

This work is supported by the Natural Science Foundation of Jilin Province, China under Grant No. YDZJ202101ZYTS149.

References

- [1] N. Hatziaargyriou, J. Milanovic, C. Rahmann, V. Ajarapu, C. Canizares, I. Erlich, D. Hill, I. Hiskens, I. Kamwa, B. Pal *et al.*, "Definition and classification of power system stability—revisited & extended," *IEEE Transactions on Power Systems*, vol. 36, no. 4, pp. 3271–3281, 2020.
- [2] E. G. Potamianakis and C. D. Vournas, "Short-term voltage instability: effects on synchronous and induction machines," *IEEE Transactions on power systems*, vol. 21, no. 2, pp. 791–798, 2006.
- [3] K. N. Hasan, R. Preece, and J. V. Milanović, "Existing approaches and trends in uncertainty modelling and probabilistic stability analysis of power systems with renewable generation," *Renewable and Sustainable Energy Reviews*, vol. 101, pp. 168–180, 2019.
- [4] J. Shair, H. Li, J. Hu, and X. Xie, "Power system stability issues, classifications and research prospects in the context of high-penetration of renewables and power electronics," *Renewable and Sustainable Energy Reviews*, vol. 145, p. 111111, 2021.
- [5] K. Kawabe and K. Tanaka, "Analytical method for short-term voltage stability using the stability boundary in the PV plane," *IEEE Transactions on Power Systems*, vol. 29, no. 6, pp. 3041–3047, 2014.
- [6] A. M. Stanković and A. T. Sarić, "Dynamic voltage stability assessment in large power systems with topology control actions," *IEEE Transactions on Power Systems*, vol. 31, no. 4, pp. 2892–2902, 2015.
- [7] H. Ge, Q. Guo, H. Sun, and W. Zhao, "A model and data hybrid-driven short-term voltage stability real-time monitoring method," *International Journal of Electrical Power & Energy Systems*, vol. 114, p. 105373, 2020.
- [8] I. Kamwa, S. Samantaray, and G. Joos, "Development of rule-based classifiers for rapid stability assessment of wide-area post-disturbance records," *IEEE Transactions on Power Systems*, vol. 24, no. 1, pp. 258–270, 2009.
- [9] S. Dasgupta, M. Paramasivam, U. Vaidya, and V. Ajarapu, "Real-time monitoring of short-term voltage stability using PMU data," *IEEE Transactions on Power Systems*, vol. 28, no. 4, pp. 3702–3711, 2013.
- [10] J. D. Pinzón and D. G. Colomé, "Real-time multi-state classification of short-term voltage stability based on multivariate time series machine learning," *International Journal of Electrical Power & Energy Systems*, vol. 108, pp. 402–414, 2019.
- [11] L. Zhu, C. Lu, and Y. Sun, "Time series shapelet classification based online short-term voltage stability assessment," *IEEE Transactions on Power Systems*, vol. 31, no. 2, pp. 1430–1439, 2015.
- [12] L. Duchesne, E. Karangelos, and L. Wehenkel, "Recent developments in machine learning for energy systems reliability management," *Proceedings of the IEEE*, vol. 108, no. 9, pp. 1656–1676, 2020.
- [13] Y. Zhang, Y. Xu, Z. Y. Dong, and R. Zhang, "A hierarchical self-adaptive data-analytics method for real-time power system short-term voltage stability assessment," *IEEE Transactions on Industrial Informatics*, vol. 15, no. 1, pp. 74–84, 2018.
- [14] Y. Zhang, Y. Xu, R. Zhang, and Z. Y. Dong, "A missing-data tolerant method for data-driven short-term voltage stability assessment of power systems," *IEEE Transactions on Smart Grid*, vol. 10, no. 5, pp. 5663–5674, 2018.
- [15] M. Lashgari and S. M. Shahrtash, "Fast online decision tree-based scheme for predicting transient and short-term voltage stability status and determining driving force of instability," *International Journal of Electrical Power & Energy Systems*, vol. 137, p. 107738, 2022.
- [16] H. Hagmar, L. Tong, R. Eriksson *et al.*, "Voltage instability prediction using a deep recurrent neural network," *IEEE Transactions on Power Systems*, vol. 36, no. 1, pp. 17–27, 2021.
- [17] W. Huang, W. Zheng, and D. J. Hill, "Distribution network reconfiguration for short-term voltage stability enhancement: An efficient deep learning approach," *IEEE Transactions on Smart Grid*, vol. 12, no. 6, pp. 5385–5395, 2021.
- [18] G. Wang, Z. Zhang, Z. Bian, and Z. Xu, "A short-term voltage stability online prediction method based on graph convolutional networks and long short-term memory networks," *International Journal of Electrical Power & Energy Systems*, vol. 127, p. 106647, 2021.
- [19] Y. Luo, C. Lu, L. Zhu, and J. Song, "Data-driven short-term voltage stability assessment based on spatial-temporal graph convolutional network," *International Journal of Electrical Power & Energy Systems*, vol. 130, p. 106753, 2021.
- [20] L. Zhu, D. J. Hill, and C. Lu, "Intelligent short-term voltage stability assessment via spatial attention rectified RNN learning," *IEEE Transactions on Industrial Informatics*, vol. 17, no. 10, pp. 7005–7016, 2020.
- [21] Y. Li, M. Zhang, and C. Chen, "A deep-learning intelligent system incorporating data augmentation for short-term voltage stability assessment of power systems," *Applied Energy*, vol. 308, p. 118347, 2022.
- [22] R. Zhang, W. Yao, Z. Shi, X. Ai, Y. Tang, and J. Wen, "Towards multi-scenario power system stability analysis: An unsupervised transfer learning method combining DGAT and data augmentation," *IEEE Trans. Power Syst.*, early access, Nov. 8, 2022. doi: 10.1109/TPWRS.2022.3220569.
- [23] A. Vaswani, N. Shazeer, N. Parmar, J. Uszkoreit, L. Jones, A. N. Gomez, Ł. Kaiser, and I. Polosukhin, "Attention is all you need," *Advances in Neural Information Processing Systems*, vol. 30, 2017.
- [24] J. Gao, Y. Chen, W. Hu, and D. Zhang, "An adaptive deep-learning load forecasting framework by integrating transformer and domain knowledge," *Advances in Applied Energy*, vol. 10, p. 100142, 2023.
- [25] M. Matar, P. G. Estevez, P. Marchi, F. Messina, R. Elmoudi, and S. Wshah, "Transformer-based deep learning model for forced oscillation localization," *International Journal of Electrical Power & Energy Systems*, vol. 146, p. 108805, 2023.
- [26] Z. Zhong, L. Guan, Y. Su, J. Yu, J. Huang, and M. Guo, "A method of multivariate short-term voltage stability assessment based on heterogeneous graph attention deep network," *International Journal of Electrical Power & Energy Systems*, vol. 136, p. 107648, 2022.
- [27] M. Zhang, J. Li, Y. Li, and R. Xu, "Deep learning for short-term voltage stability assessment of power systems," *IEEE Access*, vol. 9, pp. 29711–29718, 2021.
- [28] L. Zhu, C. Lu, Z. Y. Dong, and C. Hong, "Imbalance learning machine-based power system short-term voltage stability assessment," *IEEE Transactions on Industrial Informatics*, vol. 13, no. 5, pp. 2533–2543, 2017.
- [29] I. J. Goodfellow, J. Pouget-Abadie, M. Mirza, B. Xu, D. Warde-Farley, S. Ozair, A. Courville, and Y. Bengio, "Generative adversarial networks," *arXiv preprint arXiv:1406.2661*, 2014.

- [30] M. Arjovsky, S. Chintala, and L. Bottou, "Wasserstein generative adversarial networks," in *International Conference on Machine Learning*. PMLR, 2017, pp. 214–223.
- [31] I. Gulrajani, F. Ahmed, M. Arjovsky, V. Dumoulin, and A. Courville, "Improved training of wasserstein gans," *arXiv preprint arXiv:1704.00028*, 2017.
- [32] L. Zhu, C. Lu, and Y. Luo, "Time series data-driven batch assessment of power system short-term voltage security," *IEEE Transactions on Industrial Informatics*, vol. 16, no. 12, pp. 7306–7317, 2020.
- [33] C. Ren and Y. Xu, "A fully data-driven method based on generative adversarial networks for power system dynamic security assessment with missing data," *IEEE Transactions on Power Systems*, vol. 34, no. 6, pp. 5044–5052, 2019.
- [34] D. S. Mai and L. T. Ngo, "Semi-supervised fuzzy c-means clustering for change detection from multispectral satellite image," in *2015 IEEE International Conference on Fuzzy Systems (FUZZ-IEEE)*. IEEE, 2015, pp. 1–8.
- [35] Y. Li, J. Li, and Y. Wang, "Privacy-preserving spatiotemporal scenario generation of renewable energies: A federated deep generative learning approach," *IEEE Transactions on Industrial Informatics*, vol. 18, no. 4, pp. 2310–2320, 2022.
- [36] Y. Li, B. Wang, Z. Yang, J. Li, and C. Chen, "Hierarchical stochastic scheduling of multi-community integrated energy systems in uncertain environments via stackelberg game," *Applied Energy*, vol. 308, p. 118392, 2022.
- [37] M. Mirza and S. Osindero, "Conditional generative adversarial nets," *arXiv preprint arXiv:1411.1784*, 2014.
- [38] Y. Li, M. Han, M. Shahidehpour, J. Li, and C. Long, "Data-driven distributionally robust scheduling of community integrated energy systems with uncertain renewable generations considering integrated demand response," *Applied Energy*, vol. 335, p. 120749, 2023.
- [39] D. Chicco and G. Jurman, "The advantages of the matthews correlation coefficient (MCC) over F1 score and accuracy in binary classification evaluation," *BMC Genomics*, vol. 21, no. 1, pp. 1–13, 2020.
- [40] Q. Xu, G. Huang, Y. Yuan, C. Guo, Y. Sun, F. Wu, and K. Weinberger, "An empirical study on evaluation metrics of generative adversarial networks," *arXiv preprint arXiv:1806.07755*, 2018.
- [41] N.-T. Tran, V.-H. Tran, N.-B. Nguyen, T.-K. Nguyen, and N.-M. Cheung, "On data augmentation for GAN training," *IEEE Transactions on Image Processing*, vol. 30, pp. 1882–1897, 2021.
- [42] T. Van Cutsem, M. Glavic, W. Rosehart, C. Canizares, M. Kanatas, L. Lima, F. Milano, L. Papangelis, R. A. Ramos, J. A. dos Santos *et al.*, "Test systems for voltage stability studies," *IEEE Transactions on Power Systems*, vol. 35, no. 5, pp. 4078–4087, 2020.
- [43] G. Bu, Y. Tang, and J. Hou, "PSD-ST transient stability program user manual version 5.0," *Beijing: China Electric Power Research Institute*, 2015.
- [44] J.-K. Kim, B. Lee, J. Ma, G. Verbič, S. Nam, and K. Hur, "Understanding and evaluating systemwide impacts of uncertain parameters in the dynamic load model on short-term voltage stability," *IEEE Transactions on Power Systems*, vol. 36, no. 3, pp. 2093–2102, 2021.
- [45] X. Zhang, D. J. Hill, and Y. Song, "A load dynamic stability index for short-term voltage stability assessment and control," *IEEE Transactions on Power Systems*, vol. 38, no. 4, pp. 3304–3316, 2023.
- [46] Y. Li, S. Zhang, Y. Li, J. Cao, and S. Jia, "PMU measurements-based short-term voltage stability assessment of power systems via deep transfer learning," *IEEE Transactions on Instrumentation and Measurement*, vol. 72, pp. 1–11, 2023.
- [47] N. V. Chawla, K. W. Bowyer, L. O. Hall, and W. P. Kegelmeyer, "SMOTE: synthetic minority over-sampling technique," *Journal of Artificial Intelligence Research*, vol. 16, pp. 321–357, 2002.
- [48] G. E. Batista, R. C. Prati, and M. C. Monard, "A study of the behavior of several methods for balancing machine learning training data," *ACM SIGKDD Explorations Newsletter*, vol. 6, no. 1, pp. 20–29, 2004.
- [49] A. Alhudhaif, "A novel multi-class imbalanced eeg signals classification based on the adaptive synthetic sampling (adasyn) approach," *PeerJ Computer Science*, vol. 7, p. e523, 2021.
- [50] A. Boričić, J. L. R. Torres, and M. Popov, "Fundamental study on the influence of dynamic load and distributed energy resources on power system short-term voltage stability," *International Journal of Electrical Power & Energy Systems*, vol. 131, p. 107141, 2021.